Engineering and Technology Journal
Journal homepage: https://etj.uotechnology.edu.iq

Dynamic Characterization Assessment and Optimization of Reactive Powder Underwater Concrete

Doha M. AlSaffar [*a,b], **Basil S. Al-Shathr**[b], **Suhair K. Abed**[c]

[a] Civil Engineering Dept., Al- Iraqia University, Baghdad, 10053, Iraq.
[b] Civil Engineering Dept., University of Technology-Iraq, Alsina'a street, 10066 Baghdad, Iraq.
[c] Ministry of Construction, Housing, Municipalities and Public Works, Building Research directorate, Baghdad, 10011, Iraq.
*Corresponding author Email: bce.20.05@grad.uotechnology.edu.iq

HIGHLIGHTS

- AWA promotes fiber distribution within the concrete mix
- AWA molecules' bonding could promot fiber's impact on dynamics characterization.
- Increasing microsteel fiber (MS) content from 1% to 1.5% significantly enhances impact resistance

ARTICLE INFO

Handling editor: Mahmoud S. Al-Khafaji

Keywords:
Dynamic modulus of elasticity
Impact resistance
Underwater construction
Non-dispersive concrete
Anti-washout admixture

ABSTRACT

This study investigates the dynamic properties of Reactive Powder Underwater Concrete (RPUWC), a novel composite integrating attributes of Reactive Powder Concrete and underwater cast concrete. The study focuses on assessing the impact resistance, dynamic modulus of elasticity, rigidity, and Poisson's ratio. The influence of micro steel fibers (MS) at different volume fractions (1%, 1.25%, and 1.5%) and different anti-washout admixture (AWA) dosages (0.5 %, 0.7%, and 0.9%) are examined. The findings indicate that increasing the MS content improves crack resistance and energy absorption, resulting in a substantial 155.6% enhancement in the first crack resistance when using 1.5% MS. Additionally, ultimate resistance improves by 158%. Furthermore, there are significant increases in the dynamic and modulus of rigidity as the MS percentage rises. The impact of AWA is rather limited, with a reduction in the dynamic modulus of 18.3% for 0.7% AWA and 30% for 0.9% AWA. Likewise, the modulus of rigidity decreases by 13% for 0.7% AWA and 23.9% for 0.9% AWA. Moreover, strong positive correlations between non-destructive testing (NDT) and ASTM C 215 equations are observed. This investigation addresses a significant knowledge gap, shedding light on optimizing underwater structures' performance by comprehending their dynamic response under varied MS and AWA ratios.

1. Introduction

Subaquatic concrete structures, called Underwater concrete (UWC) structures, are subject to many environmental stresses, including the forces generated by waves, currents, and abrasive interactions with sediment and marine organisms. To ensure the enduring durability of these structures, it is imperative to gauge their ability to withstand dynamic pressures over time. The evaluation of impact resistance becomes instrumental in this regard, offering insights into the efficacy of fiber-reinforced concrete in countering the aforementioned dynamic forces. Submerged structures confront the potential of impact from various sources, such as floating debris, vessels, or accidental collisions [1-2]. This underscores the significance of impact resistance testing, which replicates these dynamic loads and grants engineers an understanding of how fiber-reinforced concrete responds to sudden forces. The capability to avert cracking or damage is paramount in ensuring the safety of marine environments and human activities reliant on these structures [3].

Furthermore, the dynamic modulus of elasticity, reflecting the stiffness and rigidity of concrete under cyclic loading conditions, becomes pivotal [4-5]. UWC structures are constantly exposed to dynamic forces stemming from waves and currents. A profound comprehension of the dynamic modulus of elasticity assists in gauging the material's resilience against these cyclic loads, signifying its potential to recover its original shape after enduring dynamic loading. This property, essential for underwater structures, plays a pivotal role in crack control and preventing damage propagation, enhancing overall structural durability [6]. The aspect of vibrations cannot be overlooked, as underwater structures are confronted with vibrations from diverse sources such as water flow, machinery, or nearby construction activities. Concrete boasting a higher dynamic modulus

http://doi.org/10.30684/etj.2023.143193.1566
Received 07 September 2023; Received in revised form 21 October 2023; Accepted 22 October 2023; Available online 29 November 2023
20232412-0758/University of Technology-Iraq, Baghdad, Iraq

of elasticity emerges as adept at dampening vibrations, thereby mitigating the risk of fatigue-induced failures and ensuring structural stability and safety [7].

Underwater structures are susceptible to shear forces attributed to wave action, water flow, and dynamic loading. Understanding the modulus of rigidity becomes a critical factor in assessing the concrete's ability to counter these shear forces, thereby averting shear-related failures that could lead to cracking and deformations [7-8]. The notion of Poisson's ratio comes into play when anticipating how a material will deform under axial or lateral loads. This comprehension is vital for designing structures capable of withstanding the forces prevalent in the marine environment. A low Poisson's ratio signifies resistance to transverse strains, effectively reducing the likelihood of cracking when confronted with lateral loads or constrained expansion. This trait aids in minimizing the risk of cracking within underwater structures subjected to diverse dynamic forces [9].

In recent years, numerous research studies have been published to enhance the properties of UWC by incorporating supplementary cementitious materials SCMs like silica fume SF, ground granulated blast furnace slag GGBFS, and fly ash FA [10-12]. Although there has been a significant increase in research efforts focused on improving underwater concrete (UWC) properties by introducing additional cementitious materials and nano-additives, the effect of adding fibers to its dynamic characteristics remains an area that hasn't been extensively investigated [13-16]. This study endeavors to bridge this knowledge gap by investigating the dynamic properties of advanced UWC, achieved by amalgamating the attributes of Reactive Powder Concrete (RPC) with those of underwater cast concrete [17].

Notably, Reactive Powder Underwater Concrete (RPUWC), a novel variant, emerges from this amalgamation. Given the scarcity of research on the influence of fiber addition on the dynamic properties of RPUWC, this investigation assumes pivotal significance, particularly in marine constructions.Owing to the paucity of research dealing with the influence of fiber addition on the dynamic properties of RPUWC, this subject assumes paramount significance, particularly in marine constructions. The present investigation aims to develop reinforced specimens' dynamic properties, incorporating three distinct volume fractions of micro steel fibers MS (1%, 1.25%, and 1.5%). In addition, all statistical analyses in this work were performed with Minitab 19.

2. Methodology

2.1 Materials Used and Mix Proportion

The raw materials utilized in the study consisted of ordinary Portland cement CEM I 42.5 [18]. 15% of micro silica fume (SF) was employed as cement replacement [19]. Silica sand with a particle size of less than 600μm was incorporated, possessing a fineness modulus of 2.75, and a specific gravity of 2.65 was used. In a powder form of natural welan gum, the anti-wash admixture AWA was used in three different dosages: 0.5%, 0.7%, and 0.9% by weight of cementitious materials [20]. A naphthalene-based high-range water reducer was employed, conforming to ASTM C494M-08 Type F [21-22] standards. The dosage percentage of the HRWRA (High-Range Water Reducer admixture) was adjusted to achieve a slump flow of 200-300mm [21,23]. The specific mixture proportions can be found in Table 1.

The chemical composition and physical specifications of the cementitious materials are listed in Table 2. For the fiber-reinforced RPUWC, various volumetric dosages of MS were mixed, specifically 0, 1, 1.25, and 1.5. The characteristics of the MS included a length of 12 mm, diameter of 0.2 mm, density of 7800 kg/m^3, and tensile strength of 2500 MPa. In the nomenclature of the mixtures, the first number indicates the AWA dosage, while the second number represents the volume fraction of fibers.

Table 1: Mix proportion of the RPUWC mixtures, kg/m^3

	Unit weight, kg/m^3							
Mixture ID	**OPC***	**SF**	**SS****	**AWA**	**HRWRA**	**Water**	**MS**	**F_cMPa**
M 0.5	850	150	935	5	22.7	230	-	69.3
M 0.5-1	850	150	935	5	22.7	230	78	73
M 0.5-1.25	850	150	935	5	22.7	230	97.5	75
M 0.5 -1.5	850	150	935	5	22.7	230	117	76.4
M 0.7	850	150	935	7	27.6	230	-	64
M 0.7-1	850	150	935	7	27.6	230	78	67.8
M 0.7-1.25	850	150	935	7	27.6	230	97.5	73.3
M 0.7-1.5	850	150	935	7	27.6	230	117	80.1
M 0.9	850	150	935	9	32.2	230	-	62
M 0.9-1	850	150	935	9	32.2	230	78	65.1
M 0.9-125	850	150	935	9	32.2	230	97.5	69.0
M 0.9-1.5	850	150	935	9	32.2	230	117	75.2

Note: OPC: ordinary Portland cement.; SF: silica fume, SS: silica sand, AWA: anti-wash admixture, MS: micro steel fiber.
*Initially, the OPC content was 1000 kg/m^3. Since 15% of the cement is replaced with SF, the new OPC content is 1000 kg/m^3 × (1 - 0.15) = 850 kg/m^3.
** SS: was 1.1 by weight of OPC.

Table 2: Chemical and physical properties of cementitious materials

Oxides,%	OPC	SF
SiO_2	21.7	94
Al_2O_3	5.48	0.5
Fe_2O_3	3.17	2
CaO	63.03	0.8
MgO	3.41	0.9
Na_2O+K_2O	0.51	1
SO_3	2.22	0.2
Specific gravity	3.15	2.2
Blain fineness, cm^2/gm	3267	200000

2.2 Mixture Preparation and Mix Sequence

In this study, RPUWC utilized 15% SF and consisted of 12 mixtures with two variable factors: AWA and MS percentages, as outlined in Table 1. For optimal performance, the AWA admixture should be added as a concentrated slurry by mixing powdered AWA with a quarter of the water and resting for 15 minutes. To expedite AWA hydration, mixing it at 75-95°C is possible. Concrete mixing involves the gradual addition of the liquid mixture, HRWRA, and hydrated AWA. The mixing sequence for RPUWC was conducted according to the procedure described by Alsaffar et al. [17]. After achieving a better consistency in the mixture, the MS was gradually added to the mixture during continued mixing, ensuring proper dispersion and mixed for an additional approximately 2 minutes after all fibers had been added. After mixing, the fresh concrete was placed in various molds for underwater casting. All specimens were taken out from those molds after 48 hr. after the initial pouring, followed by standard curing [17,24-25].

2.3 Testing Methods

In the research study, various experimental test methods were employed to evaluate the dynamic behavior of RPUWC after 28 days of curing. The tests conducted in accordance with standard guidelines were as follows:

The drop-weight test assessed the impact resistance and energy absorption capacity of RPUWC specimens, as cited by Marsh et al. [25]. Prepared and cured RPC specimens underwent controlled impact loads using a drop-weight testing machine. (63.5 mm) diameter hardened steel ball, a flat baseplate with a positioning bracket similar to that shown in Figure 1. In addition to this equipment, a mold to cast (152 mm) diameter (63.5 mm) thick. The energy absorbed during failure was carefully measured and recorded, providing valuable insights into RPUWC's dynamic response to impact loading. To determine RPUWC's dynamic properties, such as transverse, longitudinal, and torsional resonant frequencies, resonant frequency RF tests were conducted according to ASTM C 215 [26]. RPUWC specimens with 100 mm diameter and 200 mm height cylinder specimens were secured in a testing apparatus and subjected to three different mods of vibrations. The response of RPUWC specimens to the vibrations was recorded and analyzed, providing valuable data for evaluating RPUWC's potential use in structures subject to dynamic loading conditions.

(a) (b) (c)

Figure 1: Impact test setup and specimens, (a) RPWUC specimens after failure, (b) Impact test machine, (c) RPUWC specimen under test

3. Results and Discussion

3.1 Effect of AWA and MS on The Impact Resistance of RPUWC

The test setup consists of a drop tower with a vertical guide and a release mechanism for the drop weight. The specimen is securely clamped or fixed at the tower's base, as illustrated in Figures 1 and 2. The drop weight test determines the point at which the material first develops a visible crack, called the first crack (FC). The FC provides crucial information about the material's resistance to initiating cracks under impact.

In contrast, the ultimate resistance (UR) indicates the maximum force or load the material can withstand during impact before catastrophic failure occurs. This parameter reflects the material's overall toughness and energy-absorbing ability [27]. The ultimate failure in drop weight tests is when cracks in the specimen have propagated to such an extent that the pieces of concrete are in contact with at least three of the four positioning lugs on the baseplate. This criterion indicates a significant loss of structural integrity and is considered the point of failure for the material under dynamic loading conditions.

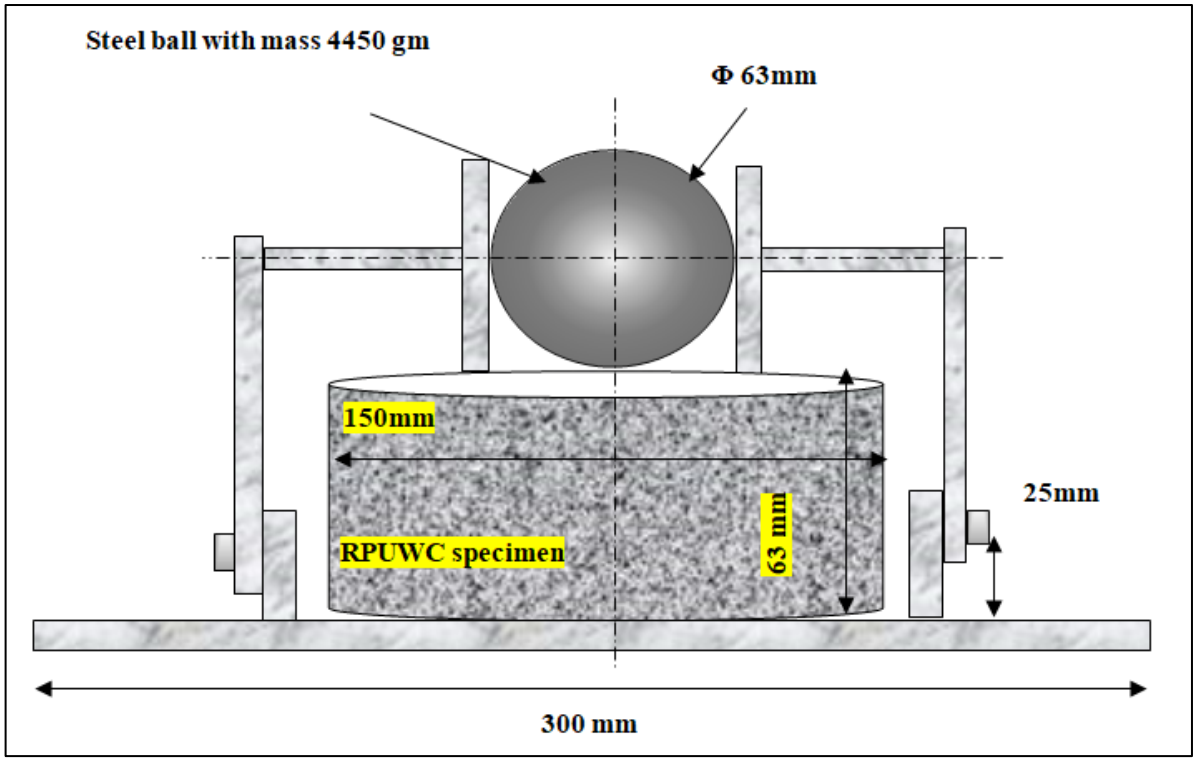

Figure 2: Sketch for RPUWC specimen under impact test

In addition to the criterion of ultimate failure, a 5-mm crack width is utilized as a specific failure requirement in certain drop weight tests, particularly for evaluating brittle materials, such as concrete. This criterion states that if a visible crack with a width of 5 mm or more is observed on the surface of the specimen during the test, it is deemed to have failed [26,28-29]. Figure 3 (a, b) presents a scatter plot of the effect of AWA and MS on the impact resistance of the RPUWC. The results indicate that adding MS contributes to an increase in the percentage enhancement of FC and UR of the RPUWC. The percentage enhancement in FC and UR refers to the delayed detection of FC and UR for reinforced RPUWC compared to RPUWC specimens without MS.

The percentage enhancement in FC and UR for different MS volume fractions (1.00%, 1.25%, and 1.50%) was observed as follows: for the 1.00% MS volume fraction, the FC% enhancement ranges from 21.3% to 62.2%, and the UR% enhancement ranges from 34% to 63%. For the 1.25% MS volume fraction, the FC% enhancement ranges from 58.8% to 113.3 %, and the UR% enhancement ranges from 68% to 117 %. For the 1.50% MS volume fraction, the FC % enhancement ranges from 91.3% to 155.6%, and the UR% enhancement ranges from 108 % to 158%. The increase in FC% and UR % enhancement with higher MS volume fractions indicates that the presence of MS contributes significantly to crack bridging and energy absorption during impact loading, leading to improved impact resistance. The percentage enhancement in FC and UR due to the addition of fiber for different AWA dosages (0.5%, 0.7%, and 0.9%) was observed as follows: For the 0.5% AWA dosage, the FC% enhancement ranges from 21.3% to 91.3%, and the UR% enhancement ranges from 34% to 108%. For the 0.7% AWA dosage, the FC% enhancement ranges from 41.9% to 101.6%, and the UR % enhancement ranges from 50% to 114%. For the 0.9% AWA dosage, the FC% enhancement ranges from 62.2% to 155.6%, and the UR% enhancement ranges from 63% to 158%. The increase in FC % and UR% enhancement with higher AWA dosages indicates that the AWA admixture improves the cohesion between the concrete constituents, resulting in better dispersion of MS and enhanced bonding between the MS and the matrix. This improved interaction leads to higher energy absorption and crack resistance. A simple linear regression analysis is used to model the relationship between the UR and FC for a set of data points, as summarized in Table 3 (A,B). The regression equation was obtained using (1) is:

$$UR = 1.34FC - 2.055 \quad (1)$$

The coefficient of determination (R-squared) is 99.22 %, which indicates that approximately 99.22% of the variability in the UR can be explained by the linear relationship with the FC. This high R-squared value suggests that the regression model fits the data well, and the FC variable is highly predictive of the UR, as shown in Figure 4. The adjusted R-squared (R-sq(adj)) is 99.14%. The adjusted R-squared accounts for the number of predictor variables in the model and is slightly lower than the

R-squared value. It penalizes the model for including unnecessary variables and provides a more conservative estimate of the goodness-of-fit.

Table 3-B presents the analysis of variance (ANOVA), which assesses the statistical significance of the regression model. The results indicate how much of the total variability in the dependent variable (UR) is explained by the linear relationship with the independent variable (FC). The regression sum of squares (SS) is 18241.8, and the mean square (MS) is 18241.8. The error sum of squares (SS) is 143.1, and the MS is 14.3. This model quantifies the variability in the data that is not accounted for by the linear relationship with FC. The F-test statistic assesses whether the regression model is statistically significant. In this case, the F-test statistic is 1274.33 with a p-value of 0.000. The extremely low p-value indicates that the regression model is highly significant and the relationship between UR and FC is not due to chance. Therefore, the null hypothesis, which states that the regression coefficients are zero, is rejected, and there is a significant linear relationship between UR and FC.

Table 3: Regression Analysis: UR versus FC

(A) Model Summary					
S	**R-sq**		**R-sq(adj)**		
3.78349	99.22 %		99.14 %		
(B) Analysis of Variance					
Source	**DF**	**SS**	**MS**	**F**	**P**
Regression	1	18241.8	18241.8	1274.33	0.000
Error	10	143.1	14.3	-	-
Total	11	18384.9	-	-	-

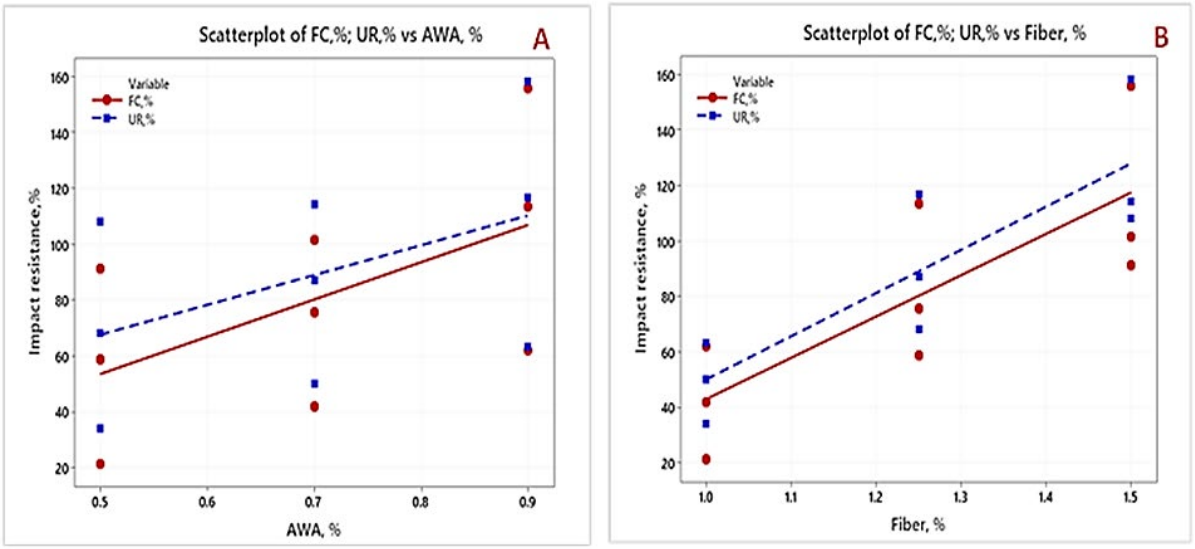

Figure 3: Effect of (A) AWA% and, (B) MS% on impact resistance of RPUWC at 28 days

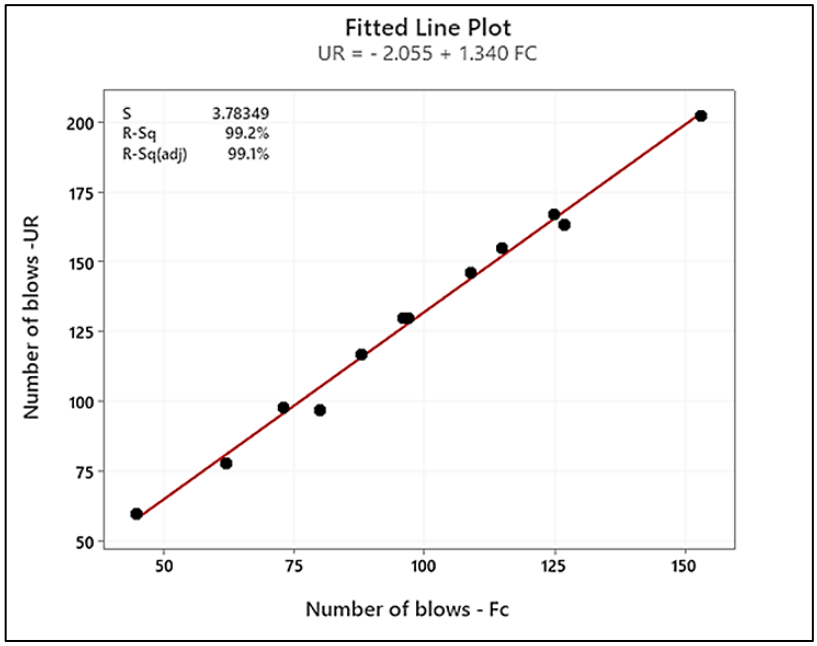

Figure 4: The relationship between FC and UR of RPUWC

3.2 Effect of Awa and Ms on Dynamic Modulus and Modulus of Rigidity of RPUWC

At least three cylindrical RPUWC specimens with a 100mm diameter and a 200 mm height are prepared for each mixture. The RF testing apparatus used is designed specifically for concrete specimens, as shown in Figure 5. The response of the concrete specimen during the test is measured using an accelerometer [26]. The recorded data is used to identify the RF for each vibrational mode (transverse, longitudinal, and torsional). The fundamental RF corresponding to the peaks in the frequency response curve is calculated, as shown in Figure 5. The dynamic moduli for the concrete specimens were determined according to ASTM C 215- 02 (2002)[26] procedures, as shown in Figure 6 (a-c).

Table 4 summarizes the dynamic modulus E, modulus of rigidity G, and Poisson's ratio (μ) of the RPUWC. These data indicate that adding MS has a noticeable effect on the dynamic modulus of elasticity (E) of the reinforced RPUWC mixtures. As the volumetric dosage of MS increases from 1% to 1.5%, there is a progressive increase in E. Mixtures with higher MS dosages, such as M 0.5-1.5 and M 0.9-1.5, have the highest values, 42.3 and 38.6 GPa, respectively. Incorporating MS in concrete results in a more interconnected and reinforced microstructure, increasing stiffness and deformation resistance. This, in turn, elevates the E, indicating the enhanced ability of the material to withstand dynamic loads and vibrations [5,29]. Including MS enhances the effective crack propagation resistance and deformation reduction under dynamic loads. Consequently, the concrete becomes stiffer and more resilient, resulting in higher E values, as shown in Figure 7A.

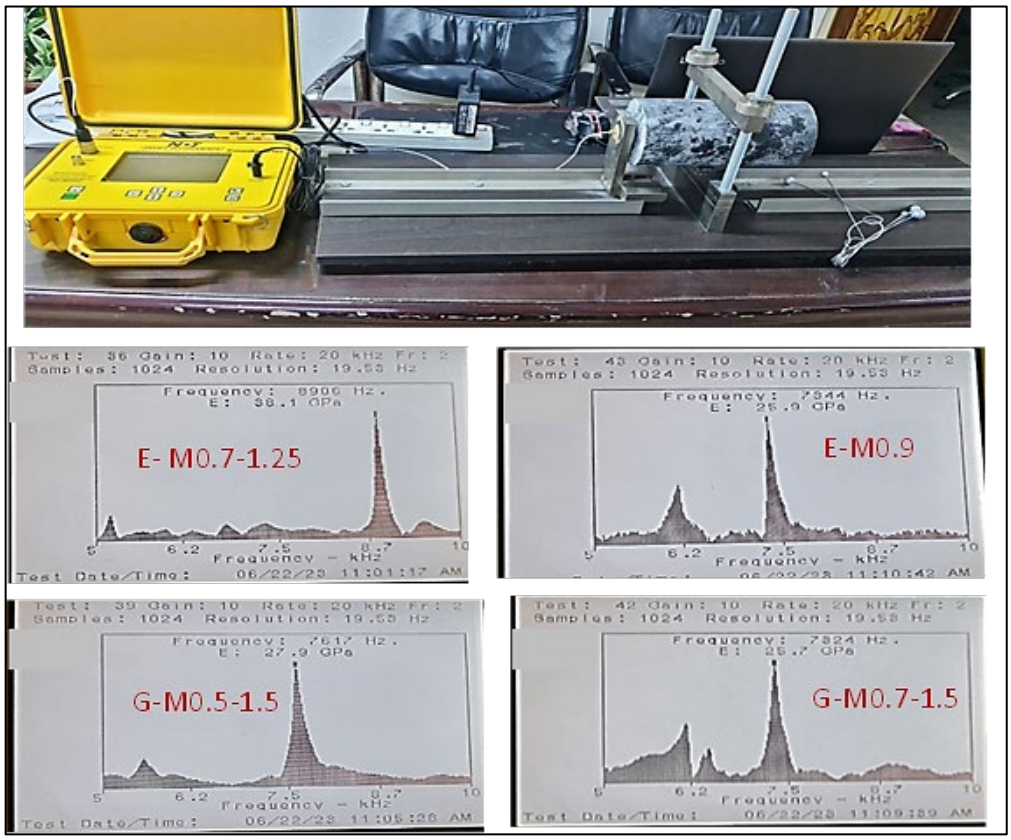

Figure 5: The resonant frequency test setup and some examples of the output resulted

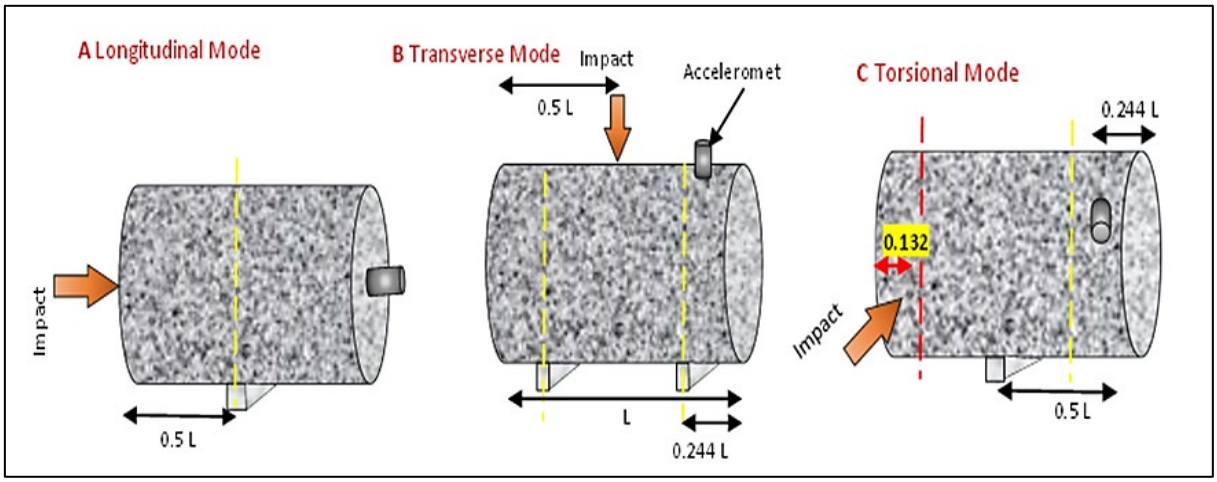

Figure 6: Sketch of resonant frequency tests of cylindrical specimens in the three modes of vibration: (A) longitudinal; (B) transverse; (C) torsional

Similar to its effect on E, adding MS also significantly impacts the G of the RPUWC mixtures. With increasing volumetric dosage of MS, there is a progressive rise in the value of G. These results concur with those of Carrillo et. Al; and Najim [7,30] a semi-uniform relationship with MS% substitution. Mixtures with higher MS dosages, such as M 0.5-1.5 and M 0.9-1.5, exhibit the highest values, 27.2 and 25 GPa, respectively. Adding MS reinforces the concrete matrix and improves its ability to resist shear stresses and deformations, resulting in higher values of G, as shown in Figure 7B.

Table 4: Compressive strength and dynamic properties of the RPUWC specimens tested by NDT

Mixture ID	F_c, MPa	E, GPa	G, GPa	G/E	Poisson's ratio
M 0.5	69.3	37	13.8	37.3	0.22
M 0.5-1	73	39.4	15.7	39.8	0.22
M 0.5-1.25	75	40.5	17	42.0	0.23
M 0.5 -1.5	76.4	42.3	18.2	43.0	0.236
M 0.7	64	30.2	12	39.7	0.216
M 0.7-1	67.8	35.3	13.2	37.4	0.22
M 0.7-1.25	73.3	38.1	15.2	39.9	0.227
M 0.7-1.5	80.1	39.9	16.8	42.1	0.23
M 0.9	62	25.9	10.5	40.5	0.216
M 0.9-1	65.1	33.5	12.6	37.6	0.227
M 0.9-125	69.0	35.2	13.7	38.9	0.23
M 0.9-1.5	75.2	38.6	16	41.5	0.235

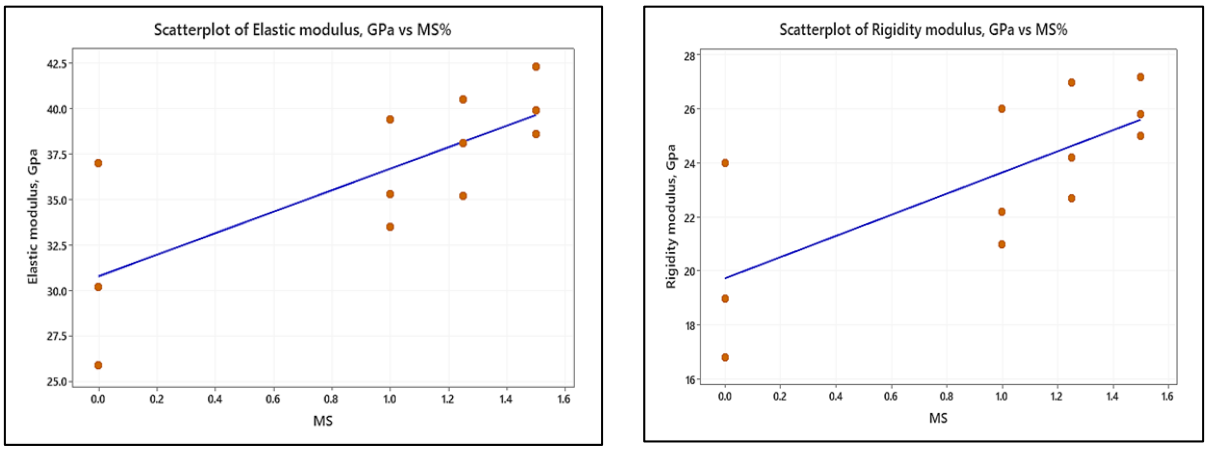

(A) **(B)**

Figure 7: Effect of MS% on (A) the dynamic modulus; (B) Modulus of rigidity of the RPUWC

The data shows some variability in E for each AWA percentage. For example, at 0.5% AWA, E ranges from 37.0 to 42.3 GPa. Similarly, at 0.7% AWA, E varies from 30.2 to 39.9 GPa. For 0.9% AWA, E varies from 25 to 38.6 GPa.

Figure 8 (A,B) show the effect of AWA on E and G of RPUWC. Significant differences in the effects can be observed compared with the previous figure that illustrates the impact of added MS on E and G. Adding 0.9% AWA reduces both E and G. In contrast, its effect appears negligible when 0.5% AWA is used. To confirm these observations, further investigations were performed to study the individual and the interaction effects of AWA and MS on the reduction ratio, utilizing statistical analysis by Minitab 19. As shown in Figure 9 (A, B), using 0.9% AWA exhibits greater effectiveness compared to using 0.7% AWA in minimizing the reduction ratio in E were 13%, 14%, and 30% for M 0.9-1, M 0.9-1.25, and M 0.9-1.5, respectively. However, the reduction percentages in E were 5.9%, 10.4%, and 18.3% for M0.7-1, M 0.7-1.25, and M 0.7-1.5, respectively. One of the goals of this study is to minimize the reduction in E% through the manipulation of the two parameters, MS and AWA, by optimizing the responses from Minitab 19, as shown in Figure 10. The optimization process successfully identifies Solution 1 with an optimal combination of 1.5% MS and 0.7% AWA, resulting in a very close match to the target value for E% reduction. These findings emphasize the significance of selecting appropriate combinations of MS and AWA to control the dynamic behavior of the concrete effectively.

These findings show that AWA promotes better fiber distribution within the concrete mix. Improved fiber distribution leads to a denser and more compact concrete matrix, increasing its strength and reducing permeability. Properly distributed fibers can enhance concrete's overall strength and energy absorption capacity. When subjected to dynamic loads, these fibers help distribute stress and prevent the propagation of cracks. A well-distributed fiber network can increase the ability of concrete to absorb and dissipate energy, making it more resistant to dynamic loads [31,32]. Moreover, AWA helps maintain a stable mix, reducing the risk of segregation [33-36]. The robust helical bonding arrangement of the welan gum molecules could potentially enhance the interfacial bonding between the cement particles and the surrounding matrix [36]. This improved bonding forms a more cohesive concrete matrix, reducing the risk of fiber disintegration in moist environments.

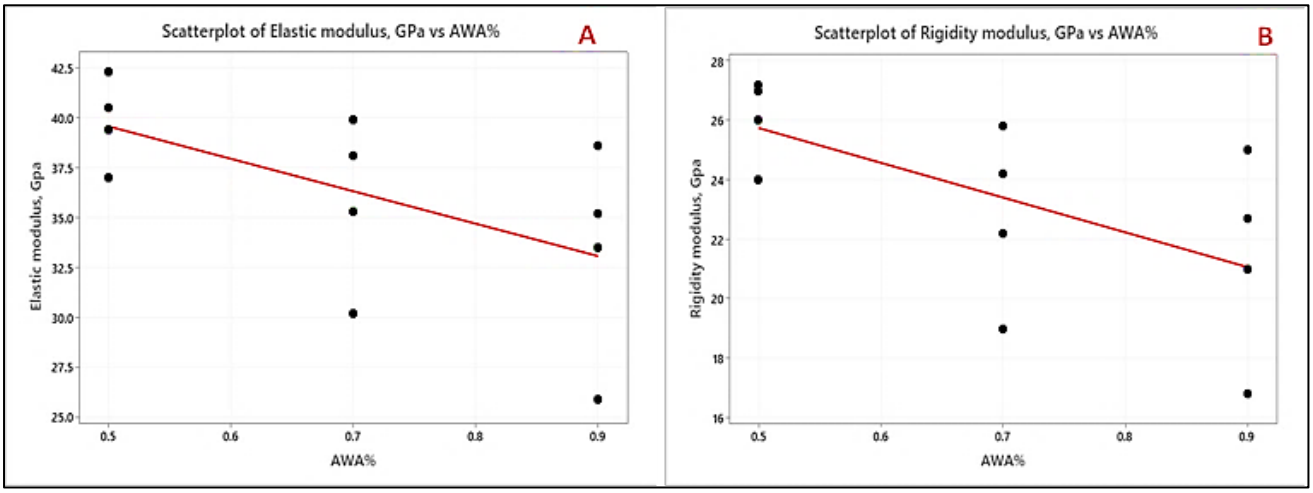

Figure 8: Effect of AWA% on (A) the dynamic modulus; (B) Modulus of rigidity of the RPUWC

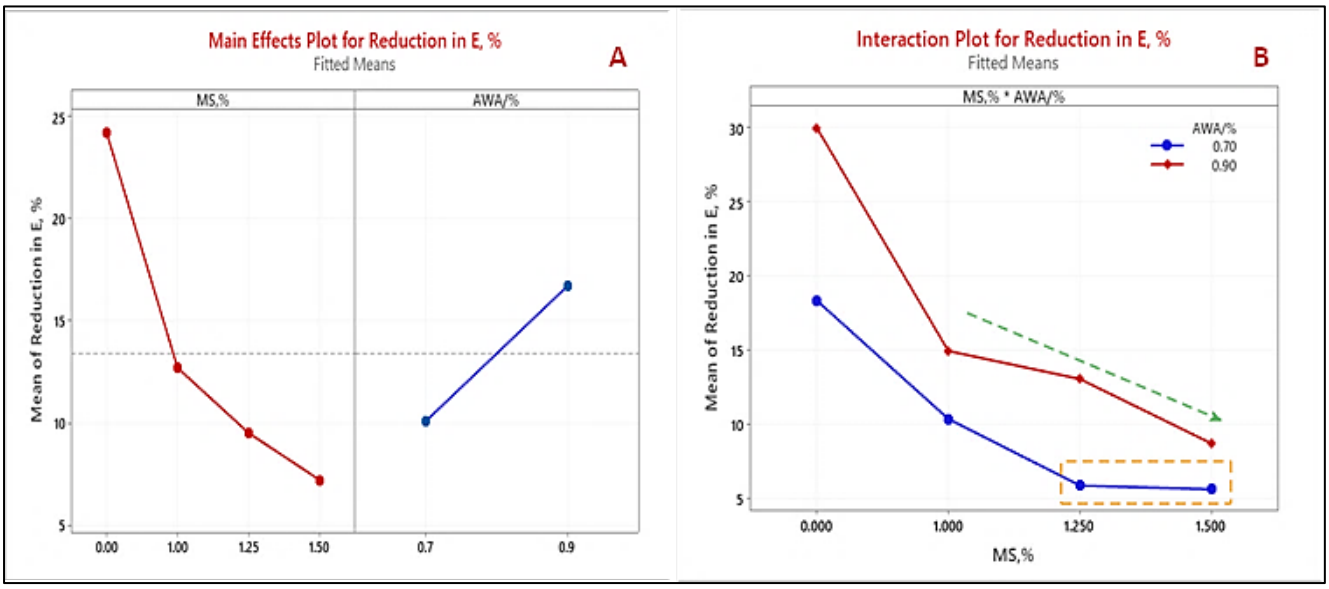

Figure 9: Effect of (A) AWA%, MS% and; (B) the interaction between AWA%*MS% on E of the RPUWC mixtures

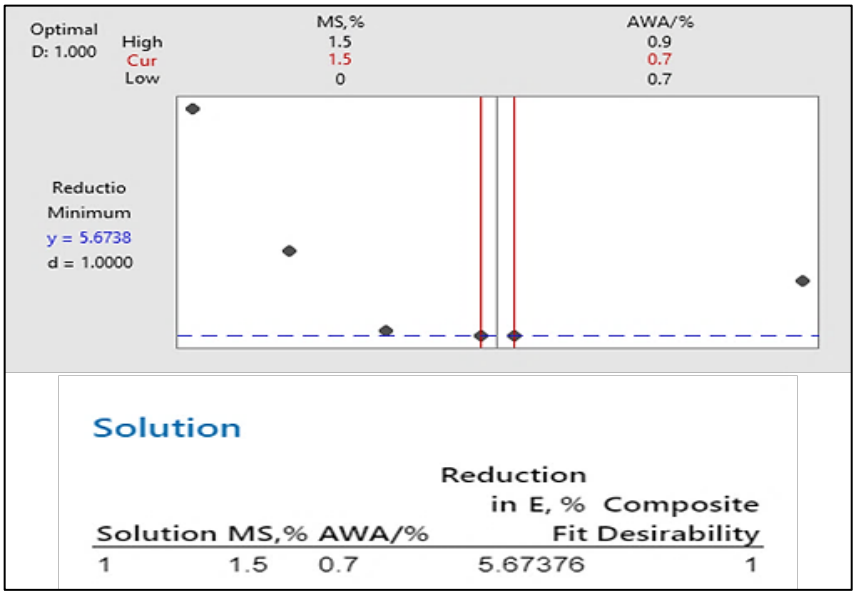

Figure 10: Response optimization of two factors AWA and MS on E of the RPUWC mixtures (Minitab output)

The modulus of rigidity measured in this study of RPUWC is presented in Table 5. The results indicate that increasing AWA to 0.7% and 0.9% leads to a reduction in G. Conversely, the addition of MS at varying percentages (1%, 1.25%, and 1.5%) significantly improves the G of the RPUWC.

To gain a more comprehensive understanding of the performance of the reinforced RPUWC, an interaction plot was generated using Minitab 19. Figure 11 (A,B) demonstrate the individual effects of MS and AWA and their interaction (MS* AWA) on G.

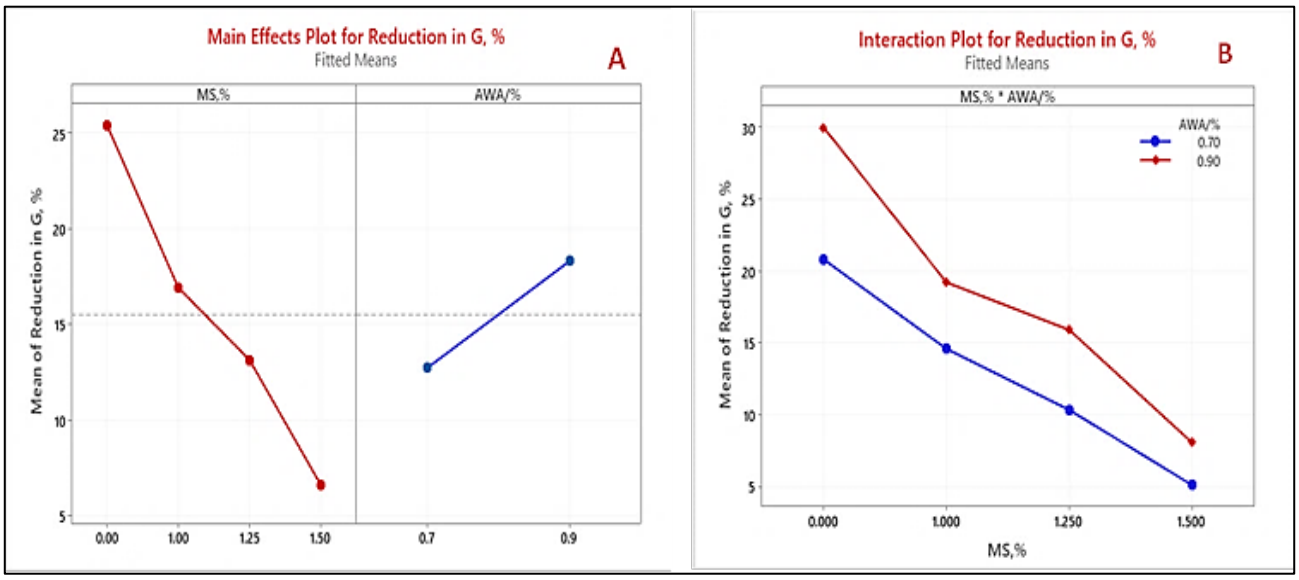

Figure 11: Effect of (A) AWA%, MS% and; (B) the interaction between AWA%*MS% on E of the RPUWC mixtures

Figure 12 shows the percentages of enhancement in the G of RPUWC due to using three volumetric dosages of MS (1%, 1.25%, and 1.5%). The enhancement values represent the increase in G compared to the reference RPUWC. These results indicate that when the fiber dosage increases from 1% to 1.5%, the enhancement in G also increases, demonstrating a positive correlation between fiber content and G improvement. Specifically, when the fiber dosage is 1%, the enhancement in G is approximately 8.33%. This shows that even a relatively low dosage of MS can notably improve the rigidity of the RPUWC. The enhancement percentages vary in specific instances within each MS dosage group. For instance, at a fiber dosage of 1%, the enhancement in G ranges from 8.33% to 16.84%, indicating some variability in the response of the concrete to the added fiber. Similarly, at a fiber dosage of 1.25%, the enhancement in G varies from 27.37% to 35.12%, whereas at an MS dosage of 1.5%, it ranges from 35.79% to 48.81%. These variations in enhancement percentages can be attributed to several factors, including the distribution of fibers in the concrete matrix, the aspect ratio of the fibers, and the overall quality of the concrete mix.

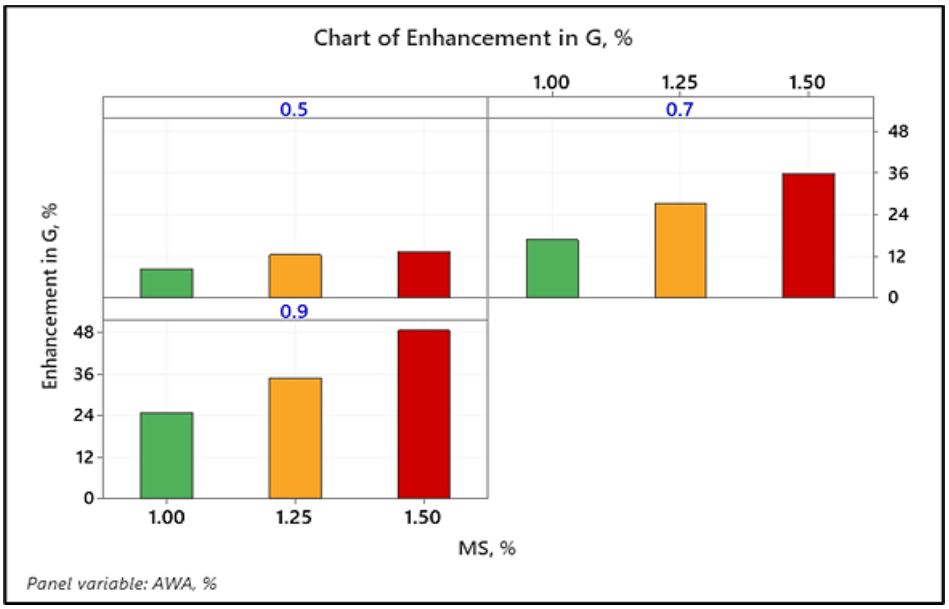

Figure 12: The impact of different AWA dosage levels on the performance of MS in terms of the modulus of rigidity (G) within the matrix of RPUWC

The mixtures containing 0.9% AWA demonstrate superior performance, exhibiting the substantial and effective influence of MS on enhancing the dynamic modulus of rigidity. Incorporating 1.5% MS results in enhancement percentages of 48.8%,

35.7%, and 13.3% compared to using 0.9%, 0.7%, and 0.5% AWA, respectively. These findings highlight the pronounced improvement in dynamic stiffness achieved with 0.9 % AWA, surpassing the enhancements observed with higher fiber contents of 1.5%. This confirms the significance of precisely tailoring the fiber dosage to maximize the dynamic mechanical properties of the RPUWC.

Figure 13 shows the output obtained from the Minitab program, which provides valuable information about the relationship between E and G. The regression equation was provided using (2):

$$E = 2.609 + 1.44G \quad (2)$$

This equation represents the linear relationship between the elastic and rigidity modulus. It indicates that a linear equation can predict the E based on G. The coefficients of the equation are 2.609 and 1.440, which indicate the intercept and the slope, respectively. The intercept represents the estimated elastic modulus when G is zero, which may not have a practical interpretation in this context.

The values of S and R-squared provide insights into the goodness-of-fit of the regression model. S measures the average distance between the observed data points and the values predicted by the model. In this case, S is 0.628855 GPa, which indicates the typical deviation of the actual elastic modulus values from the predicted values by the regression equation. Smaller values of S indicate a better fit of the model to the data. Furthermore, using the regression equation, S represents the proportion of variance in the dependent variable E explained by the independent variable G.

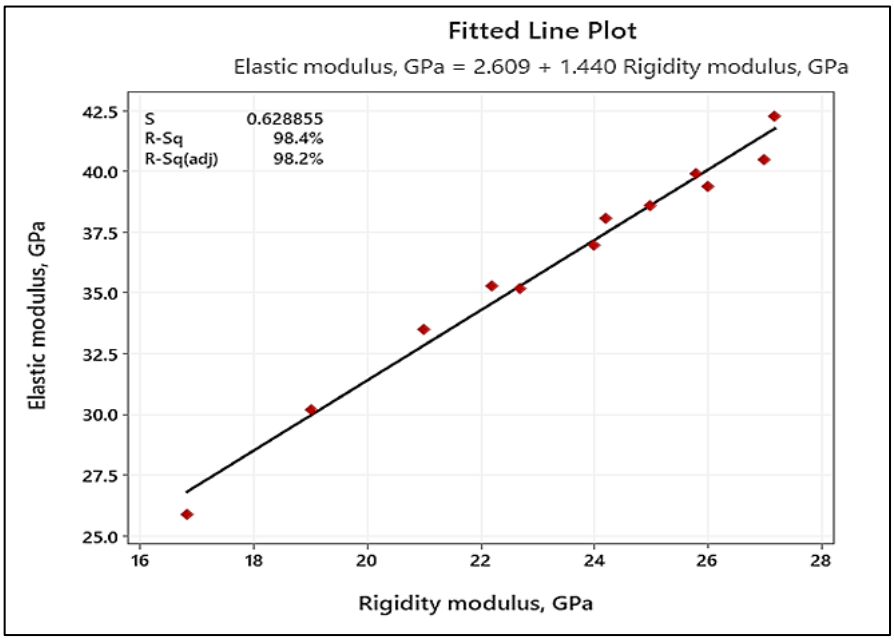

Figure 13: Fitted plot of E and G for the RPUWC mixtures

The value of R-squared is 98.36 %, which indicates that approximately 98.36% of the variability in the elastic modulus can be accounted for by the rigidity modulus in this model. However, R-squared (adjusted) is 98.19%, slightly lower than the unadjusted R-squared. In this case, the difference between R-squared and R-squared (adjusted) is small, suggesting that the model's predictive power is not significantly affected by the number of predictor variables. Table 5 summarizes the G/E values: the minimum was 37.4% for M 0.5, and the maximum was 43% for M 0.5-1.5. As stated by Malhotra and Carino [37], the rigidity modulus is about 40 % of the modulus of elasticity.

3.3 Effect of AWA and MS on E, G, and Poisson's Ratio of RPUWC by NDT

Figure 14 gives the Poisson's RPUWC ratio with different MS and AWA dosages. Generally, adding MS to RPUWC tends to increase its Poisson's ratio so that the RPUWC becomes more resistant to lateral contraction when stretched axially. This effect is attributed to the stiffness of the steel fibers, which oppose lateral contraction more effectively than plain RPUWC. If stiff fibers (e.g., micro-steel fibers) are added to the concrete mix, they increase the material's overall stiffness. In this case, the concrete becomes less compliant and more deformation-resistant [7]. As a result, the lateral contraction when the material is stretched along one axis may be reduced, leading to a higher Poisson's ratio.

The Poisson's ratio varies with different AWA dosages (0.5%, 0.7%, and 0.9%). These results indicate no clear trend in Poisson's ratio with different AWA dosages. The variations are relatively small, with Poisson's ratio ranging from 0.216 to 0.236. The trend of slightly higher Poisson's ratios with higher AWA dosages might suggest that the admixture has a minor influence on the mechanical behavior of the RPUWC. However, this effect is not as prominent as the effect of MS. Per the guidelines outlined in ACI 544.1R, fiber volume fractions below 2% are deemed to result in a Poisson's ratio equivalent to that of plain concrete. This observation aligns with the recommendations the ACI Committee 544 set forth in conjunction with the American Concrete Institute, as documented in 2008 [25].

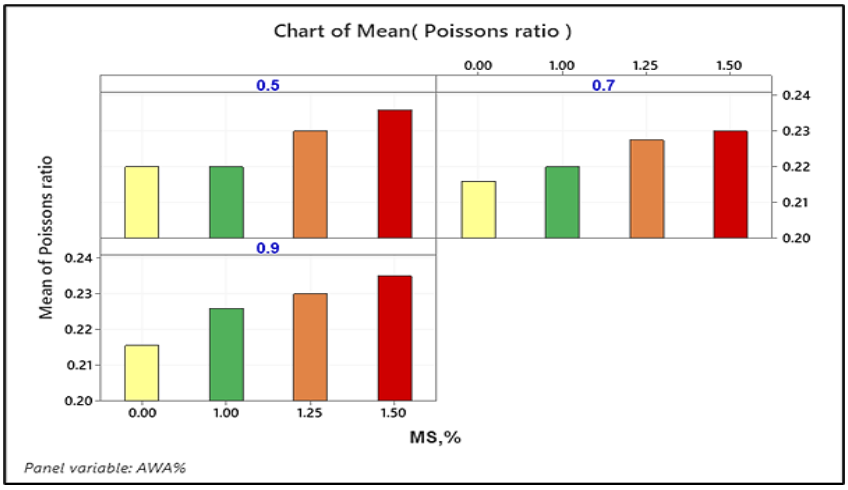

Figure 14: The impact of different AWA dosage levels on the performance of MS in terms of Poisson's ratio within the matrix of (RPUWC)

The interaction between the two factors (AWA and MS) determined using ANOVA is shown in Table 5 (A-F), which presents Poisson's ratio, compressive strength (MPa) versus AWA, and MS. This analysis determines if there are statistically significant interactions between these factors and their effects on Poisson's ratio and the compressive strength of RPUWC. ANOVA analyzes the relationship between two factors: AWA and MS. AWA have three levels: 0.5, 0.7, and 0.9 (representing the dosage percentages). MS has four levels: 0.00, 1.00, 1.25, and 1.50 (representing the dosage percentages). The F-statistic for AWA is 2.46, with a p-value of 0.166. This p-value is greater than the common significance level of 0.05. This suggests that the effect of AWA on Poisson's ratio is not statistically significant.

For the effect of MS on Poisson's ratio, the F-statistic for MS is 29.04 with a very low p-value of 0.001. This implies that there is a strong indication that the variation in Poisson's ratio can be attributed to different levels of MS. The differences in Poisson's ratio among the different MS levels are likely not due to random chance but rather a meaningful effect of the micro-steel fiber dosage. Table 5-D summarizes the model and shows that the coefficient of determination (R-squared) is 93.88%. This indicates that 93.88% of the variability in Poisson's ratio is explained by the model (AWA and MS). The adjusted R-squared, which considers the number of predictors in the model, is 88.78%. This suggests that the model effectively explains the variability in Poisson's ratio based on the dosages of AWA and MS.

Table 5-E provides the ANOVA output focused on the analysis of compressive strength (in MPa) with respect to AWA and MS. The F-statistic for AWA is 6.66, with a p-value of 0.030. This p-value is less than the common significance level of 0.05, suggesting that the effect of AWA on compressive strength is statistically significant. Meanwhile, the F-statistic for MS is 16.93, with a very low p-value of 0.002. This p-value is much lower than 0.05, indicating that the effect of MS on compressive strength is statistically significant. Thus, the variation in compressive strength can be attributed to different levels of MS dosages. The coefficient of determination (R-squared) is 91.44% (Table 5-F), indicating that 91.44% of the variability in compressive strength is explained by the model (AWA and MS). The adjusted R-squared, which considers the number of predictors, is 84.31%. This suggests that the model effectively explains the variability in compressive strength based on the dosages of AWA and MS.

Table 5: ANOVA: Poissons ratio; Compressive strength, MPa versus AWA%; MS

(A) Factor Information

Factor	Type	Levels	Values
AWA%	Fixed	3	0.5; 0.7; 0.9
MS	Fixed	4	0.00; 1.00; 1.25; 1.50

(B) Analysis of Variance for Poissons ratio

Source	DF	SS	MS	F	P
AWA%	2	0.000027	0.000014	2.46	0.166
MS	3	0.000484	0.000161	29.04	0.001
Error	6	0.000033	0.000006	-	-
Total	11	0.000545	-	-	-

(C) Analysis of Variance for Poissons ratio

Source	DF	SS	MS	F	P
AWA%	2	0.000027	0.000014	2.46	0.166
MS	3	0.000484	0.000161	29.04	0.001
Error	6	0.000033	0.000006	-	-
Total	11	0.000545	-	-	-

(D) Model Summary

S	R-sq	R-sq(adj)
0.0023566	93.88%	88.78%

(F) Model Summary

S	R-sq	R-sq(adj)
2.18913	91.44%	84.31%

(E) Analysis of Variance for Compressive Strength, MPa

Source	DF	SS	MS	F	P
AWA%	2	63.79	31.894	6.66	0.030
MS	3	243.40	81.133	16.93	0.002
Error	6	28.75	4.792	-	-
Total	11	335.94	-	-	-

Figure 15 shows the effect of MS and AWA on the longitudinal, transverse, and torsional RF results for RPUWC. The longitudinal and transverse RF tends to decrease as the AWA percentage increases. This trend suggests that a higher percentage of AWA is associated with reducing the stiffness and mechanical integrity of the concrete specimens [15, 39].

There is a clear pattern: the combination effect between MS and AWA as MS percentage increases, the torsional RF of the concrete specimens tends to rise. This correlation suggests that a high-volume fraction of MS might enhance the ability of the concrete to resist torsional forces, resulting in increased torsional stiffness. This observation could be related to the role of AWA in improving the cohesiveness of the concrete mix, leading to better interlocking of fibers and enhanced mechanical performance. Furthermore, the reinforcement effect of MS likely hinders crack propagation and enhances the overall structural integrity of the concrete, resulting in higher torsional RF [7]. From the longitudinal and transverse RF data, increasing MS content tends to result in RF. This indicates that a higher percentage of MS enhances the flexural stiffness of the concrete and its ability to withstand bending forces, potentially due to the reinforcing effect of the fibers on crack resistance.

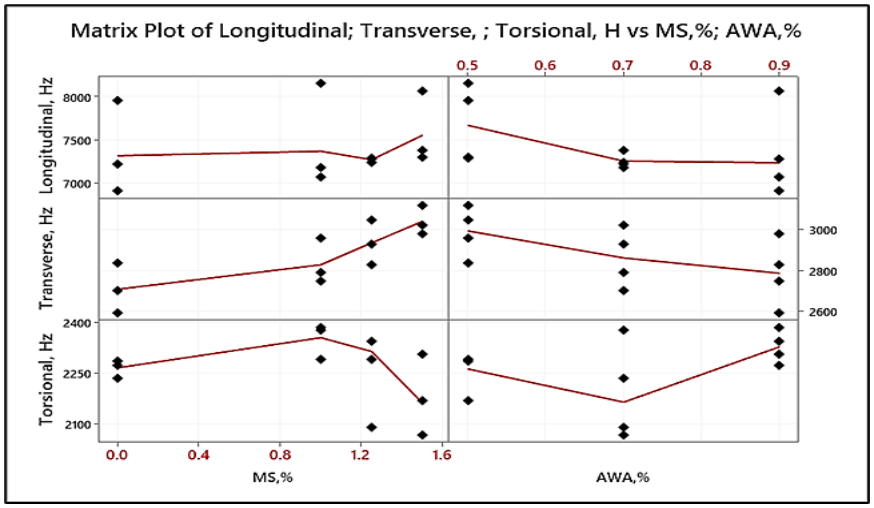

Figure 15: The effect of MS% and AWA% on the longitudinal, transverse, and torsional RF results for the RPUWC

Moreover, the percentage of enhancement in the longitudinal RF for RPUWC containing 0.5% of AWA is 2.63% for M 0.5-1. In contrast, the longitudinal RF in M 0.5-1.25 and M 0.5-1.5 is lower than that of the reference specimen, as shown in Figure 16. The percentages of reduction were 8.34% and 8.27% for M 0.5-1.25 and M 0.5-1.5, respectively. This difference could be due to the interaction between the fibers, their distribution, and the concrete matrix, leading to changes in the dynamic behavior that are not necessarily linearly correlated with fiber content at low AWA.

This behavior differs if the AWA content increases; the results indicate that the percentages of enhancement in the longitudinal RF were 0.67 %, 0.25%, and 2.22 % for RPUWC containing 0.7 % of AWA for M 0.7-1, M 0.7-1.25, and M 0.7-1.5, respectively. A noticeable improvement in the longitudinal RF appears when 0.9 % AWA is used in the RPUWC. Adding 1% MS seems to contribute to a slight improvement in the longitudinal dynamic response of the concrete of 2.42%. The percentage enhancement of approximately 5.45% for the longitudinal RF at 1.25 % MS content indicates a more pronounced increase in dynamic stiffness than the reference specimens. The percentage enhancement of approximately 16.89% for the longitudinal RF at 1.5% MS content represents a substantial increase in dynamic stiffness. Adding 1.5% MS results in a notable improvement in the deformation resistance of the concrete and its ability to maintain structural integrity under dynamic loads. as illustrated in Figure 16.

As for the results related to the transverse RF, the highest enhancement in the dynamic properties of the RPUWC is observed when 0.9% AWA is added, as illustrated in Figure 17. The percentages of enhancement were 6 %, 9.19%, and 15.03 % for M 0.9-1, M 0.9-1.25, and M 0.9-1.5, respectively. The improvement rates of RPUWC containing 0.7 % of AWA are 3.29 %, 8.48%, and 11.79% for M 0.7-1, M 0.7-1.25, and M 0.7-1.5, respectively. Figure 18 represents the interaction effect between AWA and MS on torsional RF. This result indicates that the torsional RF increased by approximately 4.57 % due to adding 1% MS. The results represent a significant increase of about 14.53% in the torsional RF with the inclusion of 1.5 % MS, and this increase is particularly noticeable when 0.5% AWA is also used.

Figure 19 includes a response optimization and prediction of enhancement percentages for torsional, transverse, and longitudinal RF of the RPUWC. The goal for each response is to maximize the enhancement percentage. These enhancement percentages represent the improvements in dynamic stiffness due to adding MS. The optimal solution will be based on the response optimization. The solution consists of two parameters: “MS” and “AWA”. Additionally, the output displays the calculated enhancement percentages for torsional, transverse, and longitudinal RF. The optimal values of MS and AWA are 1.5% and 0.9%, respectively.

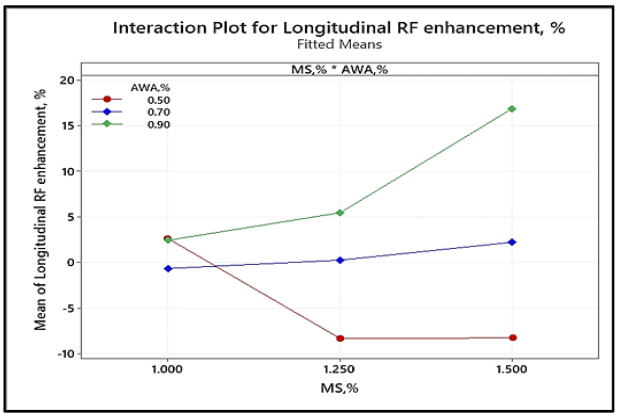

Figure 16: The interaction plot of AWA and MS for longitudinal RF enhancement

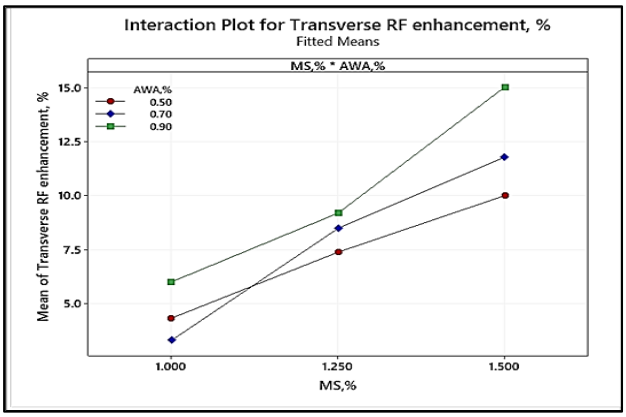

Figure 17: The interaction plot of AWA and MS for transverse RF enhancement

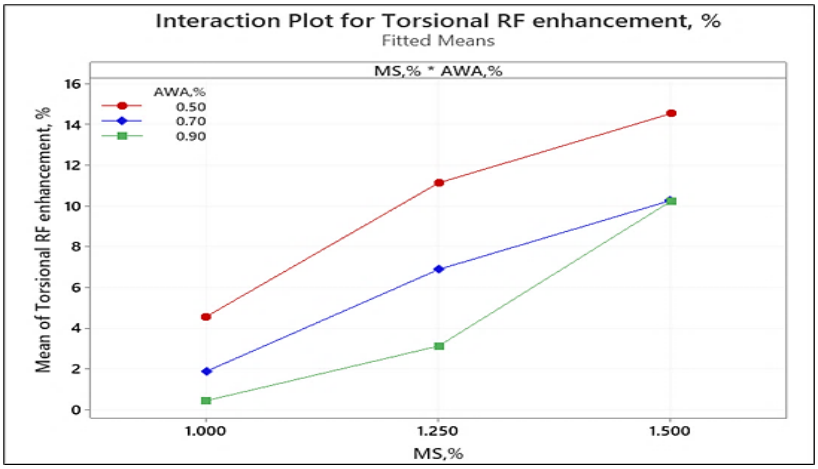

Figure 18: The interaction plot of AWA and MS for torsional RF enhancement

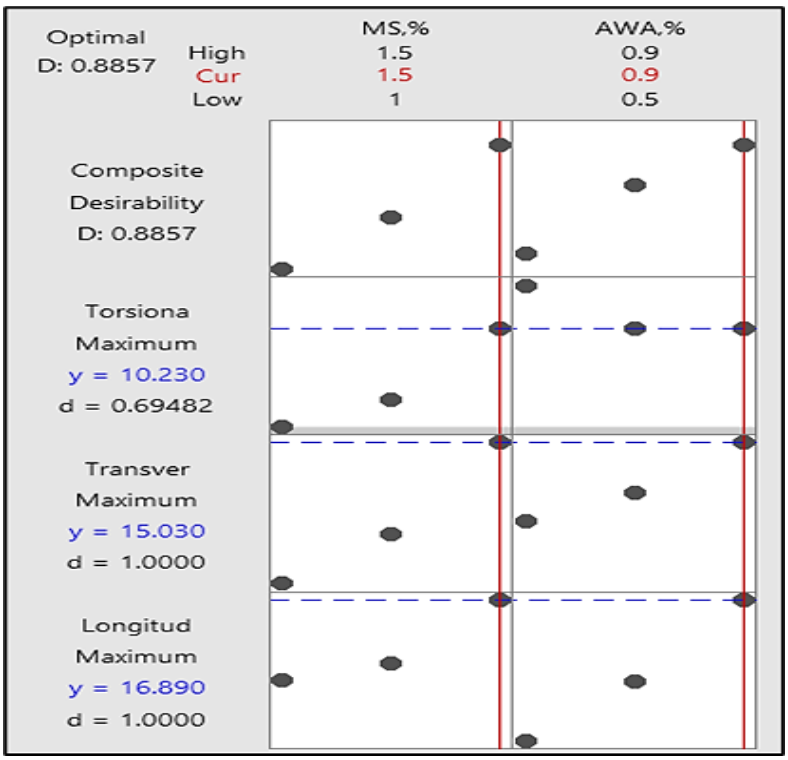

Figure 19: The response optimization and prediction of enhancement percentages for torsional, transverse, and longitudinal RF of the RPUWC (Minitab output)

3.4 Comparison Analysis of RPUWC Non-Destructive Testing (NDT) vs. ASTM C 215 Equations

The RF for the RPUWC cylinder was conducted according to ASTM C 215 equations [26]. Table 6 shows the longitudinal, transverse, and torsional RF results tested at 28 days and measured to the nearest 10 Hz as per the standard. However, Table 7 shows the dynamic properties of the RPUWC calculated by ASTM C 215 equations.

Table 6: The resonant frequency of the RPUWC specimens tested by NDT

Mixture ID	Longitudinal resonant frequency, Hz	Transverse resonant frequency, Hz	Torsional resonant frequency, Hz
M 0.5	7949	2837	2287
M 0.5-1	8157	2960	2391
M 0.5-1.25	7287	3046	2542
M 0.5 -1.5	7291	3121	2620
M 0.7	7218	2702	2236
M 0.7-1	7170	2791	2278
M 0.7-1.25	7236	2931	2390
M 0.7-1.5	7378	3020	2466
M 0.9	6899	2590	2275
M 0.9-1	7066	2746	2285
M 0.9-125	7275	2828	2346
M 0.9-1.5	8061	2979	2508

Table 7: The dynamic properties of the RPUWC calculated by ASTM C 215 equations

Mixture ID	E, GPa	G, GPa	G/E	Poisson's ratio
M 0.5	32	13.3	41.2	0.21
M 0.5-1	35	14.5	41.4	0.25
M 0.5-1.25	37	16.5	44.2	0.31
M 0.5 -1.5	39	17.6	44.7	0.35
M 0.7	29	12.5	43.4	0.18
M 0.7-1	31	13.1	42.3	0.20
M 0.7-1.25	34	14.5	42.2	0.25
M 0.7-1.5	37	15.5	42.3	0.28
M 0.9	26	12.9	48.9	0.17
M 0.9-1	30	13.1	43.9	0.19
M 0.9-125	32	13.9	43.6	0.22
M 0.9-1.5	36	16.0	44.9	0.28

Figures 20,21 and 22 represent the correlation between E NDT vs. E 215, GNDT vs. G 215, and μ NDT vs. μ 215. The results indicated that the Pearson correlation coefficient is 0.962 for E NDT vs. E215 by Minitab program. The Pearson correlation coefficient (also denoted as "r") is a statistical measure that quantifies the strength and direction of the linear relationship between two continuous variables. It ranges from -1 to +1, where -1 represents a perfect negative correlation, +1 represents a perfect positive correlation, and 0 indicates no linear correlation is close to +1, indicating a strong positive linear relationship between the two variables. 0.962 is close to +1, indicating a strong positive linear relationship between the two variables. This implies that as one variable increases, the other variable also tends to increase, and vice versa. The strength of the correlation coefficient (close to +1) indicates a high degree of consistency in the pattern of changes between these two variables. In other words, higher values of " E NDT " are typically associated with higher values of "E 215," and lower values of the elastic modulus are associated with lower values of "E 215." Additionally, a correlation coefficient 0.962 suggests that the relationship between these two variables is quite linear. This means that a scatter plot of the data points would likely show a relatively tight cluster that follows a straight-line pattern as shown in Figure 20. On the other hand, Figure 21 represents a correlation analysis between two variables: G NDT and G 215. The Pearson correlation coefficient is given as 0.930. This value is also close to +1, indicating a strong positive linear relationship between the two variables. As for results related to μ NDT vs. μ215, the Pearson correlation coefficient is given as 0.714. While not as strong as the previous correlations, the correlation still indicates a meaningful connection between the two parameters, as shown in Figure 22.

Moreover, Figure 23 related a probability plot for comparing E NDT and E 215. The mean, standard deviation, sample size (N), and Anderson-Darling statistic (AD) are measures used to assess how well a sample of data fits a particular distribution, often used for testing whether a given data set follows a specific theoretical distribution, such as the normal distribution, and the p-value is given for each dataset. The mean is 36.32, and the standard deviation is 4.677. These measures provide insights into the central tendency and spread of the data. The (AD) is 0.388, and the p-value is 0.328. These values are often used to test the hypothesis that the data follows a normal distribution. A low AD statistic and a high p-value suggest that the data will likely follow a normal distribution. The relatively high p-value (0.328) supports the notion that the dataset for E NDT might follow a normal distribution. For the second dataset related to E215, the mean is 33.24, and the standard deviation is 3.841. These values provide information about the central tendency and variability of the data. The (AD) is 0.146, and the p-value is 0.953. These values indicate that the dataset will likely follow a normal distribution. The high p-value (0.953) suggests strong evidence that the data for E 215 is normally distributed. Based on the provided probability plot and the associated statistics, both datasets E NDT and E 215 show indications of following a normal distribution. This assessment is based on the p-values and the AD statistics.

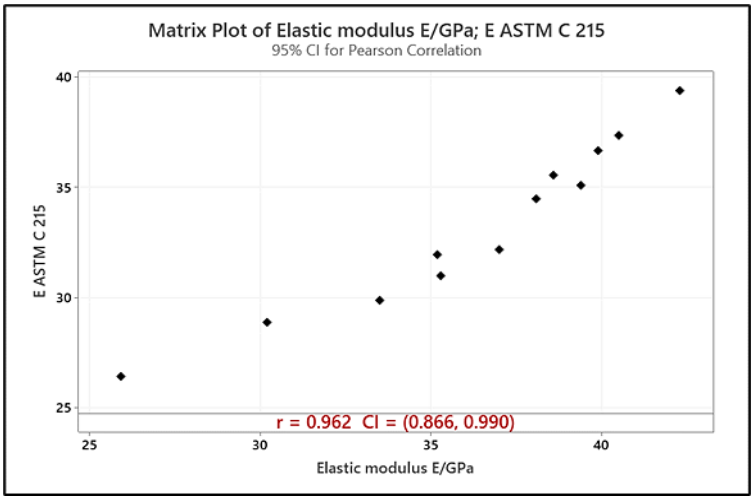

Figure 20: The correlation between E by NDT and E calculated byASTM C215 equations

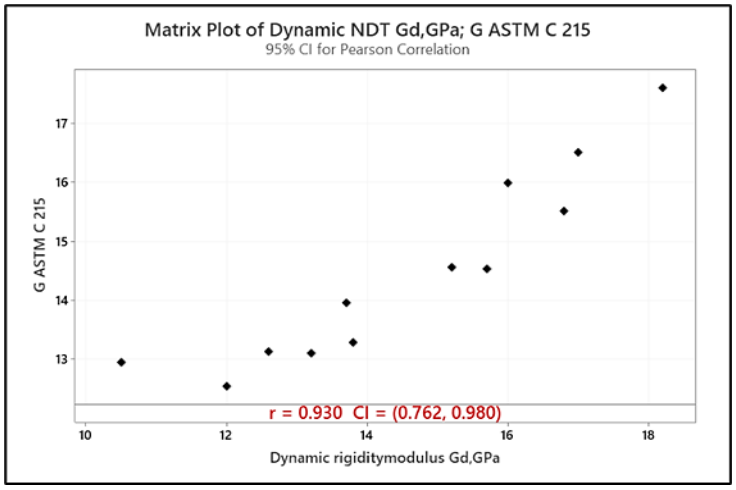

Figure 21: The correlation between G by NDT and G calculated by ASTM C 215 equations

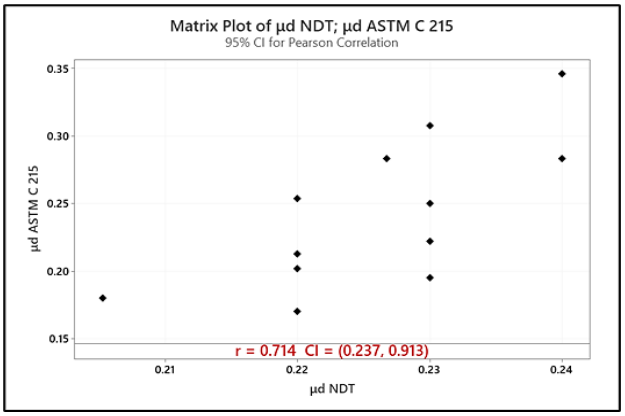

Figure 22: The correlation between Poisson's ratio by NDT and Poisson's ratio calculated by ASTM C 215 equations

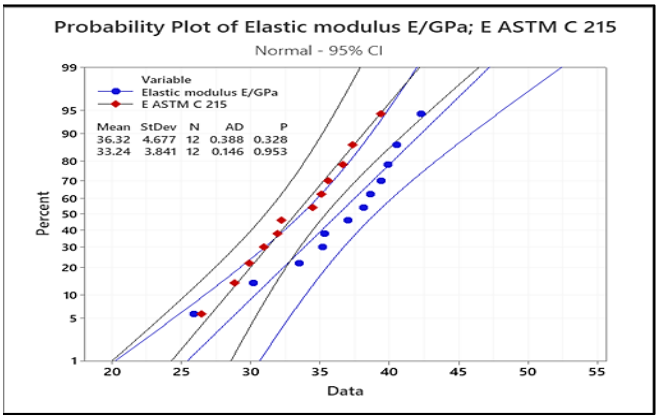

Figure 23: The probability plot for E by NDT and E calculated by ASTM C 215 equations

Similarly, the probability plot in Figure 24 associated statistics assesses whether the datasets follow a normal distribution for G $_{NDT}$ and G125. The first dataset, G $_{NDT,}$ shows the mean is 14.56, and the standard deviation is 2.297. These measures provide insights into the central tendency and spread of the data. The (AD) is 0.166, and the p-value is 0.919. The high p-value suggests strong evidence that the data for G $_{NDT}$ is likely to follow a normal distribution. The second dataset, G 215, represents a mean of 14.46 and a standard deviation 1.623. These values provide information about the central tendency and variability of the data. The AD is 0.406, and the p-value is 0.295. The p-value is relatively high, indicating that the data for G125is likely to follow a normal distribution. The statistical implications of the provided probability plot for the comparison of μ_{NDT} and μ_{215} are shown in Figure 25. The first data set for μ_{NDT} provides a mean of 0.2260, and the standard deviation is 0.009679. These

measures describe the central tendency and spread of the data. The (AD) is 0.523, and the p-value is 0.144. The relatively high p-value suggests that the data for μ_{NDT} will likely follow a normal distribution. While the second data set for μ_{215} represents, the mean is 0.2421, and the standard deviation is 0.05470. These values provide information about the central tendency and variability of the data. The (AD) is 0.239, and the p-value is 0.718. The p-value is relatively high, indicating that the data for μ_{215} will likely follow a normal distribution.

Comparing the p-values and Anderson-Darling statistics across the three datasets, it seems that the datasets related to E NDT and G 215 have p-values closer to 1 and lower AD, indicating a strong fit to normality. On the other hand, the dataset for μ NDT and μ 215 has slightly lower p-values and higher AD, suggesting a relatively good but less strong fit to normality compared to the other two datasets.

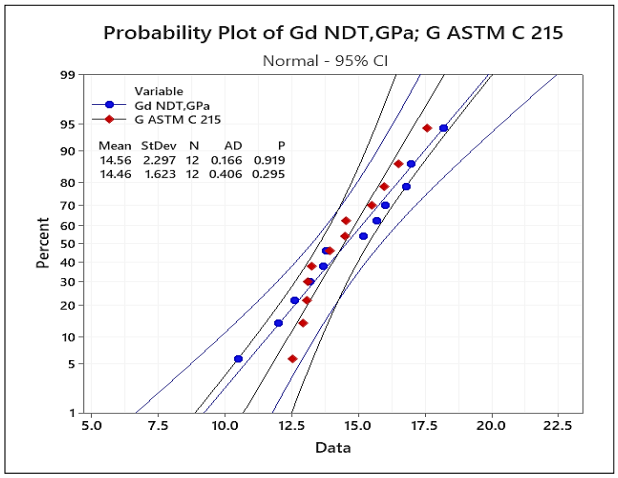

Figure 24: The probability plot for G by NDT and G calculated by ASTM C215 equations

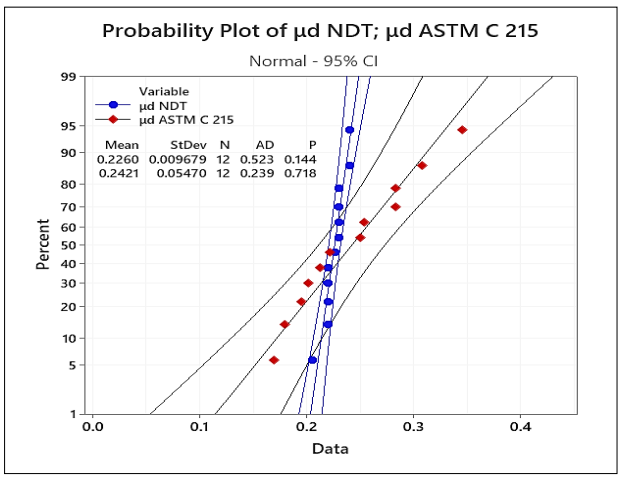

Figure 25: The probability plot for Poisson's ratio by NDT and Poisson's ratio calculated by ASTM C215 equations

4. Conclusions

Based on the findings and analysis presented earlier, the following conclusions can be made:

1) Increasing MS volume fractions from 1% to 1.5% led to higher (FC) and (UR) percentages. FC enhancement ranged from 21.3% to 155.6%, UR enhancement from 34% to 158%. MS contributed to crack bridging and energy absorption, boosting impact resistance.
2) The maximum enhancement in FC and UR was observed when using 0.9% AWA, the FC% enhancement ranges from 62.2% to 155.6%, and the UR % enhancement ranges from 63% to 158%
3) Statistical linear regression analysis supported the FC-UR relationship (UR = 1.340 FC - 2.055) with an R-squared of 99.22% and adjusted R-squared of 99.14%, highlighting the predictive power of FC for UR. The ANOVA indicated a highly significant model (p-value = 0.000).
4) The addition of MS led to a notable increase in both dynamic modulus and modulus of rigidity. Dynamic modulus showed enhancements ranging from 8.33% to 48.81% with increasing MS content from 1% to 1.5%. Similarly, modulus of rigidity exhibited improvements in the range of 8.33% to 16.84% at 1% MS dosage and up to 48.8% at 1.5% MS content. However, AWA's effect on these properties was relatively limited, with changes often overshadowed by MS's influence.
5) Addition of MS leads to an increase in Poisson's ratio, signifying enhanced resistance to lateral contraction during axial stretching. While Poisson's ratio exhibits slight variations with different AWA dosages (0.5%, 0.7%, 0.9%), no distinct trend emerges. Values range between 0.216 and 0.236, suggesting AWA's limited influence on RPUWC's mechanical behavior compared to MS.
6) The effect of AWA% and MS % on the resonant frequencies (RF) of RPUWC. With increasing AWA%, longitudinal and transverse RF tend to decrease, indicating reduced concrete stiffness and mechanical integrity. Notably, an interesting correlation emerges: higher AWA% and MS % lead to elevated torsional RF. This suggests that greater AWA concentration, coupled with higher MS fraction, enhances concrete's resistance to torsional forces, bolstering torsional stiffness. Response optimization aims to maximize enhancement percentages while adhering to specified limits. Optimal values for "MS%" and "AWA%" are found to be 1.5% and 0.9%, respectively, showcasing a strategy to enhance dynamic stiffness in RPUWC.
7) The correlation between NDT results and ASTM C 215 equations was examined for longitudinal, transverse, and torsional RF. Strong positive linear relationships were observed between NDT and ASTM C 215 for E (correlation coefficient of 0.962), indicating consistent behavior. Similarly, G showed a strong positive correlation of 0.930. While μ exhibited a slightly weaker but meaningful connection with a correlation coefficient of 0.714.

Author contributions

Conceptualization, D. AlSaffar, B. Al-Shathr and S. Abed; methodology, D. AlSaffar; validation, D. AlSaffar; investigation, D. AlSaffar; resources, D. AlSaffar, B. Al-Shathr and S. Abed; writing—original draft preparation, D. AlSaffar; writing—review and editing, B. Al-Shathr and S. Abed, supervision, B. Al-Shathr and S. Abed; project administration, B. Al-Shathr and S. Abed. All authors have read and agreed to the published version of the manuscript.

Funding

This research received no specific grant from any funding agency in the public, commercial, or not-for-profit sectors. Data availability statement Not applicable.

Data availability statement

The data that support the findings of this study are available on request from the corresponding author.

Conflicts of interest

The authors do not have a conflict of interest..

References

[1] K. H. K. Joseph J. Assaad, Yehia Daou, Simulation of Water Pressure on Washout of Underwater Concrete Repair, ACI Mater. J., 106 (2009) 529-536. https://doi.org/10.14359/51663336

[2] W. Yan, W. Cui, and L. Qi, Simulation of underwater concrete movement in flowing water using DEM-CFD coupling method, Constr. Build. Mater., 319 (2022). https://doi.org/10.1016/j.conbuildmat.2021.126134

[3] J. Lai, W. Sun, S. Xu, and C. Yang, Dynamic properties of reactive powder concrete subjected to repeated impacts, ACI Mater. J.,110 (2013) 463–472. https://doi.org/10.14359/51685793

[4] S. Giner, V T Baeza, F J Ivorra and Ó. Zornoza, E Galao, Effect of steel and carbon fiber additions on the dynamic properties of concrete containing silica fume, J. Mater., 34 (2012) 332–339. https://doi.org/10.1016/j.matdes.2011.07.068

[5] F. J. Giner, V T Ivorra, S Baeza and B. Zornoza, E Ferrer, Silica fume admixture effect on the dynamic properties of concrete, Constr. Build. Mater., 25 (2011) 3272–3277. https://doi.org/10.1016/j.conbuildmat.2011.03.014

[6] A. M. Heniegal, A. A. El Salam Maaty, and I. S. Agwa, Simulation of the behavior of pressurized underwater concrete, Alexandria Eng. J., 54 (2015) 183–195. https://doi.org/10.1016/j.aej.2015.03.017

[7] J. Carrillo, J. Ramirez, and J. Lizarazo-marriaga, Modulus of elasticity and Poisson ' s ratio of fi ber-reinforced concrete in Colombia from ultrasonic pulse velocities, J. Build. Eng., 23 (2018) 18–26. https://doi.org/10.1016/j.jobe.2019.01.016

[8] T. Wei, Huinan Liu and Y. Zhou, Ao Zou, Dujian Li, Toughening static and dynamic damping characteristics of ultra-high performance concrete via interfacial modulation approaches, Cem. Concr. Compos., 136 (2022) 104879. https://doi.org/10.1016/j.cemconcomp.2022.104879

[9] W. H. Lai, Transient dynamic response of submerged sphere shell with an opening subjected to underwater explosion, Ocean Eng., 34 (2007) 653–664. https://doi.org/10.1016/j.oceaneng.2006.06.008

[10] A. I. Jubeh, D. M. Al Saffar, and B. A. Tayeh, Effect of recycled glass powder on properties of cementitious materials contains styrene butadiene rubber, Arab. J. Geosci., 12 (2019). https://doi.org/10.1007/s12517-018-4212-0

[11] B. A. Tayeh, D. M. Al Saffar, A. S. Aadi, and I. Almeshal, Sulphate resistance of cement mortar contains glass powder, J. King Saud Univ. - Eng. Sci., 32 (2019) 495-500. https://doi.org/10.1016/j.jksues.2019.07.002

[12] B. A. Tayeh, D. M. Al Saffar, A. S. Aadi, and I. Almeshal, Sulphate resistance of cement mortar contains glass powder, J. King Saud Univ. - Eng. Sci., 32 (2019) 495-500. https://doi.org/10.1016/J.JKSUES.2019.07.002

[13] Y. Wang, L. Gu, and L. Zhao, Beneficial Influence of Nanoparticles on the Strengths and Microstructural Properties of Non-dispersible Underwater Concrete, KSCE J. Civ. Eng., 25 (2021) 4274–4284. https://doi.org/10.1007/s12205-021-1471-1

[14] J. Wang, S. Jiang, E. Cui, W. Yang, and Z. Yang, Strength gain monitoring and construction quality evaluation on non-dispersible underwater concrete using PZT sensors, Constr. Build. Mater., 322 (2022) 126400. https://doi.org/10.1016/j.conbuildmat.2022.126400

[15] M. Ali Sikandar, N. R. Wazir, M. A. Khan, H. Nasir, W. Ahmad, and M. Alam, Effect of various anti-washout admixtures on the properties of non-dispersible underwater concrete, Constr. Build. Mater., 245 (2020) 118469. https://doi.org/10.1016/j.conbuildmat.2020.118469

[16] J.-G. Baluch, Khaqan Baluch, Sher Q. Yang, Hyung-Sik Kim and S. Kim, Jong-Gwan Qaisrani, Non-Dispersive Anti-Washout Grout Design Based on Geotechnical Experimentation for Application in Subsidence-Prone Underwater Karstic Formations, Materials (Basel)., 14 (2021)1587. https://doi.org/10.3390/ma14071587

[17] D. M. Al-Saffar, B. S. Al-Shathr, and S. K. Abed, Evaluating Fresh Properties of Non-Dispersive Reactive Powder Concrete: A Novel Approach, Math. Model. Eng. Probl., 10 (2023) 1324–1332.https://doi.org/10.18280/mmep.100426

[18] M. Soutsos and P. Domone, Portland cements, in Construction Materials, Fifth edition. | Boca Raton : CRC Press, [2017]: CRC Press, 137–154, 2017. https://doi.org/10.1201/9781315164595-16

[19] ASTM C 1240-03, Standard specification for use of silica fume as a mineral admixture in hydraulic-cement concrete, mortar, and grout, ASTM Int., 15 (2003) 1–6.

[20] 546.2R-10: Guide to Underwater Repair of Concrete. 2010.

[21] N. Otsuki, M. Hisada, S. Nagataki, and T. T. Kamada, An Experimental Study on the Fluidity of Antiwashout Underwater Concrete, ACI Mater. J., 93 (1996) 20–25. https://doi.org/10.14359/9792

[22] K. H. Khayat and A. Yahia, Effect of Welan Gum-High-Range Water Reducer Combinations on Rheology of Cement Grout, ACI Mater. J., 94 (1997) 365-372. https://doi.org/10.14359/321

[23] K. Baluch, S. Q. Baluch, H.-S. Yang, J.-G. Kim, J.-G. Kim, and S. Qaisrani, Non-Dispersive Anti-Washout Grout Design Based on Geotechnical Experimentation for Application in Subsidence-Prone Underwater Karstic Formations, Materials (Basel)., 14 (2021) 1587. https://doi.org/10.3390/ma14071587

[24] H. Y. Moon and K. J. Shin, Evaluation on steel bar corrosion embedded in antiwashout underwater concrete containing mineral admixtures, Cem. Concr. Res., 36 (2006) 521–529. https://doi.org/10.1016/j.cemconres.2005.09.014

[25] H. Y. Moon and K. J. Shin, Frost attack resistance and steel bar corrosion of antiwashout underwater concrete containing mineral admixtures, Constr. Build. Mater., 21(2007) 98–108. https://doi.org/10.1016/j.conbuildmat.2005.06.050

[26] C. H. Marsh, Henry N. Woolridge, J. F. Ball, Claire Batson, Gordon B. Burnett, Eric F.P. Criswell, Marvin E. Davis, Frank H. Fekete, Frank W. Fernon, Price Forsyth, Robert B. Godfrey, Howard J. Henager, R. L. Henry, G. C. Hoff, and G. Horeczko, Measurement of Properties of Fiber Reinforced Concrete, ACI J. Proc., 75 (1978) 433–439. https://doi.org/10.14359/10941

[27] ASTM Standard C215, Standard Test Method for Fundamental Transverse , Longitudinal , and Torsional Resonant Frequencies of Concrete Specimens, ASTM Stand., 1–7, 2008, https://doi.org/10.1520/C0215-19

[28] M. Mastali and A. Dalvand, The impact resistance and mechanical properties of self-compacting concrete reinforced with recycled CFRP pieces, Compos. Part B Eng., 92 (2016) 360–376. https://doi.org/10.1016/j.compositesb.2016.01.046

[29] W. J. Cantwell and J. Morton, The impact resistance of composite materials — a review, Composites, 22 (1991) 347–362. https://doi.org/10.1016/0010-4361(91)90549-V

[30] A. El-Newihy, P. Azarsa, R. Gupta, and A. Biparva, Effect of Polypropylene Fibers on Self-Healing and Dynamic Modulus of Elasticity Recovery of Fiber Reinforced Concrete, Fibers, 6 (2018) 9. https://doi.org/10.3390/fib6010009

[31] K. B. Najim and M. R. Hall, Mechanical and dynamic properties of self-compacting crumb rubber modified concrete, Constr. Build. Mater., 27 (2012) 521–530. https://doi.org/10.1016/j.conbuildmat.2011.07.013

[32] K. Pan, R. C. Yu, G. Ruiz, X. Zhang, Á. De La Rosa, and Z. Wu, Evolution of the FPZ in steel fiber-reinforced concrete under dynamic mixed-mode loading, Constr. Build. Mater., 377 (2022) 131110. https://doi.org/10.1016/j.conbuildmat.2023.131110

[33] S. Grzeszczyk, K. Jurowski, K. Bosowska, and M. Grzymek, The role of nanoparticles in decreased washout of underwater concrete, Constr. Build. Mater., 203 (2019) 670–678. https://doi.org/10.1016/j.conbuildmat.2019.01.118

[34] Kamal H. Khayat; Mohammed Sonebi, Effect of Mixture Composition on Relative Strength of Highly Flowable Underwater Concrete, ACI Mater. J., 98 (2001) 289–295. https://doi.org/10.14359/10278

[35] M. Sonebi and K. H. Khayat, Effect of Mixture Composition on Relative Strength of Highly Flowable Underwater Concrete, ACI Mater. J., 98 (2001) 233–239. https://doi.org/10.14359/10278

[36] S. R. Abid, A. N. Hilo, N. S. Ayoob, and Y. H. Daek, Underwater abrasion of steel fiber-reinforced self-compacting concrete, Case Stud. Constr. Mater., 11 (2019) e00299. https://doi.org/10.1016/J.CSCM.2019.E00299

[37] V. R. S. De Silva, P. G. Ranjith, M. S. A. Perera, B. Wu, and T. D. Rathnaweera, The Influence of Admixtures on the Hydration Process of Soundless Cracking Demolition Agents (SCDA) for Fragmentation of Saturated Deep Geological Reservoir Rock Formations, Rock Mech. Rock Eng., 52 (2019) 435–454. https://doi.org/10.1007/s00603-018-1596-9.

[38] V. M. Malhotra and V. Sivasundaram, Resonant frequency methods, Handb. Nondestruct. Test. Concr., 1–7, 2004.

[39] K. H. Khayat, Effects of Antiwashout Admixtures on Properties of Hardened Concrete, ACI Mater. J., 93 (1996) 134–146. https://doi.org/10.14359/1412